Additively Manufactured Millimeter-Wave Dual-Band Single-Polarization Shared Aperture Fresnel Zone Plate Metalens Antenna

Jianfeng Zhu, *Member, IEEE*, Yang Yang, *Senior Member, IEEE*, Mengze Li, David McGloin, Shaowei Liao, *Senior Member, IEEE*, Jaim Nulman, *Senior Member, IEEE*, Minoru Yamada, and Francesca Iacopi *Senior Member, IEEE*

***Abstract*— Fresnel zone plate (FZP) lens antenna, consisting of a set of alternative transparent and opaque concentric rings arranged on curvilinear or flat surfaces, have been widely used in various fields for sensing and communications. Nevertheless, the state-of-art FZP lens antennas are limited to a single band due to the frequency-dependent feature, which hinders their use in multi-band applications. In this work, a shared-aperture dual-band FZP metalens antenna is proposed by merging two single-band FZP metalens antenna operating at distinct frequency bands seamlessly into one. Instead of using conventional metallic conductors, double-screen meta-grids are devised in this work to form the concentric rings. Because the meta-grids show distinct transmission/reflection properties at different frequencies, the performance of one set of concentric rings operating at the one band will not be affected by the other operating at the different band. In addition, to compensate for the phase shift introduced by the meta-grids, an additional dielectric ring layer is added atop the FZP taking advantage of additive manufacturing. Thus, the radiation performance of the dual-band FZP lens antenna is comparable to that of each single FZP metalens antenna. For proof-of-concept, an antenna prototype operating at the dual-band, 75 GHz and 120 GHz with a frequency ratio of 1.6, is fabricated using an integrated additively manufactured electronics (AME) technique. The measured peak gains of 20.3 dBi and 21.9 dBi are achieved at 75 GHz and 120 GHz, respectively.**

***Index Terms*— Fresnel zone plate (FZP), metalens antenna, additive manufacturing, dual-band, millimeter-wave (mm-wave).**

I. Introduction

Millimeter-wave (mm-wave) and terahertz (THz) technologies create a new era of many emerging research areas, such as high-resolution imaging, high-speed big data communications, and ubiquitous sensing [1-6]. Since the mm-wave spectrum is located between the microwave and optical regions, its development provides an opportunity to consolidate and reconcile the paradigms of microwave engineering with optics and photonics [7-9]. Nevertheless, the general hurdles of mm-wave technology are the tremendous loss and the quasi-optical propagation path of communication link [10]. In addition, mm-wave signals also experience extra atmospheric attenuation as compared with lower electromagnetic (EM) frequencies. As a result, mm-wave communications are mainly restricted to line-of-sight (LOS). To tackle these challenges, large-scale antenna arrays are tightly packed in the transceiver front-end to compensate for the high path loss and bridge the gap of link budget, albeit rather bulky. As an alternative approach, lenses or transmitarrays that can collimate the EM-waves from the source are used to obtain highly-directional beams. Over the last decade, various kinds of mm-wave lenses and transmitarrays based on the concept of metasurface have been proposed to meet the requirement of different mm-wave application scenarios [11-24]. Nevertheless, to achieve flexible phase control over a broad span covering the range $[-\pi, \pi]$ of the wavefront, the "meta-atoms" are usually implemented by cascading several resonant cells in a multilayered form with bonding process. Moreover, many state-of-art mm-wave metalenses and transmitarrays are limited to a single band [15-22]. To achieve dual-band feature, most of the metalenses or transmitarrays use orthogonal polarization for phase control over two bands [23-26]. Dual-band single-polarization mm-wave metalenses and transmitarrays are rarely reported because it is difficult for the "meta-atoms" to achieve dual-band/multi-band phase control of the wavefront independently in a single polarization. As for prototyping, state-of-the-art mm-wave lenses and transmitarrays use printed circuit board (PCB) to fabricate each layer independently and stacked them together. 3-D printing, also known as additive manufacturing, has offered a new and economical way to build the lenses and transmitarrays. Various kinds of lenses have been proposed using additive manufacturing [27-40]. Nevertheless, most of them are dielectric-based. In fact, state-of-the-art works using additive manufacturing are either dielectric printing (coated with metal if required) or directly metal printing. Lenses or transmitarrays using conductive and dielectric integrated additively manufactured electronics (AME) technique has not been reported. However, the one-stop integrated printing can provide more design freedom, i.e. both metallic and dielectric

Manuscript received XX, 2020. This work was supported by Nano Dimension under a PhD scholarship agreement and UTS FEIT Blue Sky Grant. (Corresponding author: Yang Yang yang.yang.au@ieee.org)

Jianfeng Zhu, Yang Yang, Mengze Li, David McGloin, and Francesca Iacopi are with School of Electrical and Data Engineering, University of Technology Sydney, Ultimo, NSW 2007, Australia (e-mail: yang.yang.au@ieee.org)

Shaowei Liao is with Guangdong Principle Key Laboratory of Millimeter-wave and Terahertz, School of Electronic and Information Engineering, South China University of Technology, Guangzhou 510641, China.

Minuro Yamada and Jaim Nulman are with Nano Dimension, 13798 NW 4th Street, Suite 315, Sunrise, FL 33325, USA.

Francesca Iacopi is also with Australian Research Council Centre of Excellence in Transformative Meta-Optical Systems, School of Electrical and Data Engineering, University of Technology Sydney, NSW 2007, Australia.

structure can be printed simultaneously without post-processing procedure such as bonding, alignment, and coating.

Fresnel zone plate (FZP) lens antenna, implemented by a set of alternative transparent and opaque concentric rings either transmitting or blocking the incident EM wave, has the advantages of a thinner profile and lighter weight than a traditional lens antenna with a drawback of 50% back reflection of energy [41-47]. Generally, each zone of the FZP lens antenna is divided into an even number of subzones. The radii (Ri) of each transparent and opaque zone can be determined by using [47]:

$$R_i = \sqrt{i\lambda_0 F + (\frac{i\lambda_0}{2})^2}, i = 1, 2, ...N \quad (1)$$

where λ_0 is the design wavelength, F is the focal length. Because of spatial dispersion, the diffraction of the FZP lens antenna is frequency-dependent. Thus, a conventional FZP lens antenna can only support a single operating bandwidth. A reconfigurable FZP lens antenna at the microwave region was proposed by using pin diodes to control different states of metasurface to realize dual-band operation [45], but still, only one diffractive pattern can generate on the aperture at a given state. In addition, the cut-off frequency of the lossy pin diodes hinders the concept from being applied to the mm-wave regions.

In this paper, a shared-aperture dual-band single-polarization FZP metalens antenna is proposed. Two sets of concentric opaque rings of FZP metalens antennas operating at low-band and high-band are formed by using double-screen meta-grids, which show distinct transmission/reflection properties at two bands. Then, they are merged in the same aperture seamlessly without affecting each other. Taking advantage of additive manufacturing, an additional dielectric ring layer is added atop the FZP to compensate for the phase shift introduced by the meta-grids. Thus, the radiation performance of the dual-band FZP lens antenna is comparable to that of each single FZP metalens antenna. For proof-of-concept, a dual-band FZP metalens antenna operating at 75 GHz and 120 GHz is fabricated using an integrated AME technique. The performance of the FZP metalens antenna has been experimentally verified. It is noted that the design is only chosen as a demonstrative example, and it has the potential to be configured to other frequencies with different frequency ratios.

II. Dual-Band FZP Lens Antenna Design

A. Antenna Geometry

The basic geometry and concept are illustrated in Figs. 1 (a) and (b). The proposed dual-band single-polarization FZP metalens antenna is realized by merging two single-band FZP metalens antennas operating at distinct frequency bands into a shared aperture. Since the radii of the concentric rings of two FZP metalens antennas are different, simply placing the rings together will destroy the performance of FZP metalens antenna at both bands. Therefore, instead of using conventional metallic conductors, the concentric rings of two FZP metalens antennas are realized by using different double-screen meta-grids (grid-A and grid-B), as shown in Fig. 1 (a). In this way, the opaque concentric rings of the high-band FZP metalens (formed by grid-B) can reflect the EM-waves at the high-band while allowing the EM-waves at the low-band to pass. Similarly, the opaque concentric rings of the low-band FZP metalens (formed by grid-A) can reflect the EM-waves at the low-band while allowing the EM-waves at the high-band to pass. Once these opaque concentric rings are combined to form the dual-band FZP metalens, there are four different regions on the aperture of the dual-band FZP metalens, namely, Region I: the overlapped area of grid-A and grid-B, presented by fully conductive layers, reflects the EM-wave at both bands. Region II: An opaque area (grid-B) reflects high-band waves, while keeps low-band waves transmitted. Region III: An opaque area (grid-A) reflects low-band waves, while keeps high-band waves transmitted. Region IV: The transparent area (neither grid-A nor grid-B exists) for waves at both bands transmitting through the metalens, as depicted in Fig. 1 (a). Thus, for the high-band, the transparent part (allowing EM-wave to pass) is formed by region III and region IV. Similarly, the transparent part is formed by region II and region IV for the low-band, as depicted in Figs. 1 (c) and (d).

B. Meta-grids Design

The crucial factor determining the performance of the proposed dual-band FZP metalens antenna is the double-screen meta-grids (grid-A and grid-B) forming concentric rings operating at low-band and high-band, as shown in Fig. 2 (a) and (b), respectively. EM-simulations are carried out in ANSYS HFSS with periodical boundary conditions (PBC). As we know, the function of the meta-grids is determined by the period between the parallel grid element. If the meta-grid period is long compared to the wavelength, the meta-grid functions as a diffraction grating and diffracts both *x*- and *y*- polarizations [48]. However, when the meta-grid spacing is much smaller than the wavelength, the meta-grid functions as a polarizer reflecting incident waves with polarization parallel to the meta-grid, and transmits the EM-wave of the orthogonal polarization. Here, the period of the meta-grid is smaller than the wavelength at low-band (75 GHz) and the grid-A functions as the polarizer to reflect the EM-waves along *y*-direction at low-band with transmission magnitude as low as around 0.1, as shown in Fig. 3 (a). While at high-band (120 GHz), the double-screen meta-grid functions as an anti-reflection coating with improved transmission magnitude reaching 0.88, demonstrating it allows the high-band EM-wave to pass. Nevertheless, the double-screen meta-grids also introduce phase abruption into the high-band transmission phase, making it 76° difference compared to the transmission phase of the one without grids-A (region IV) at 120-GHz, as seen from Fig. 3 (b). Since region IV and region III (forming by grid-A) are both transparent for the EM-waves

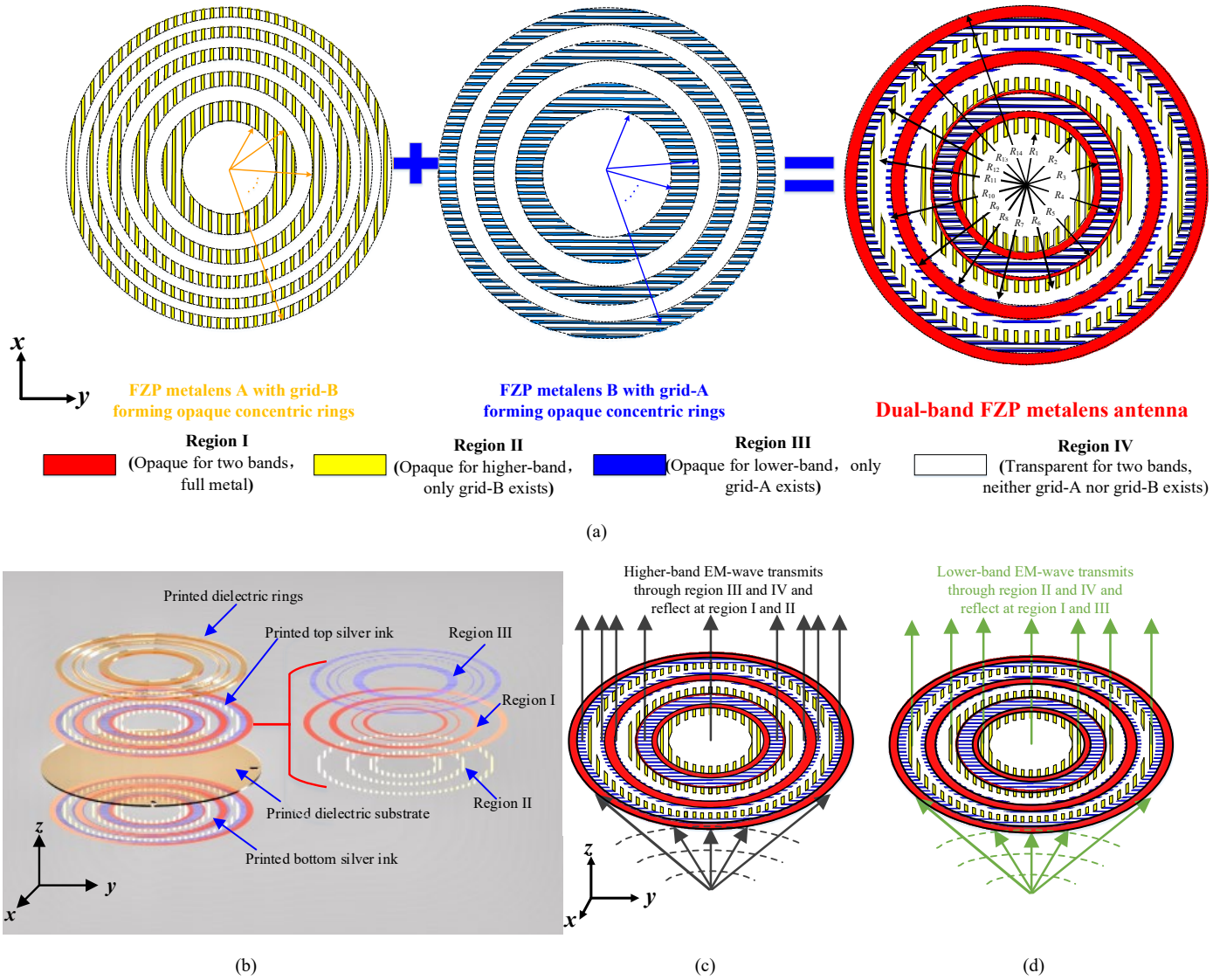

Fig. 1. (a) The design concept of the proposed dual-band FZP metalens antenna, which is implemented by merging two single-band FZP metalens antennas (FZP metalens A: operating at the high-band and FZP metalens B: operating at the low-band. R_1= 8.75 mm, R_2=11.13 mm, R_3=12.5 mm, R_4=15.4 mm, R_5=16 mm, R_6=18 mm, R_7=19.9 mm, R_8=20.34 mm, R_9=22.5 mm, R_{10}= 23.32 mm, R_{11}=24.5 mm, R_{12}=26.45 mm, R_{13}=28.21 mm, R_{14}= 29.5 mm). (b) Configurations of the proposed dual-band FZP lens antenna. (not scaled in z-direction). (c) High-band *y*-polarized EM-wave transmits through the region III and region IV and reflected at the region I and region II. (d) Low-band *y*-polarized EM-wave transmits through the region II and region IV and reflected at the region I and region III.

at high-band, additional phase compensating is required, enabling two regions to have the same transmission phase. Taking advantage of additive manufacturing, a dielectric layer with a thickness of 0.65 mm is added atop of the grids-A for phase compensating. After adding the phase-compensating dielectric layer, the transmission magnitude only slightly shifts to a higher frequency while the transmission phase of region III and region IV become nearly the same at 120-GHz, as shown in Fig. 3 (b).

As for region II, although the configuration of grid-B forming region II is similar to grid-A, the reflection principle is different. The reflection of *y*-polarized incident waves is based on half-wavelength resonance, i.e. the width of the grids is about half of the dielectric wavelength at high-band. Thus, it can reflect the EM-waves at high-band and allow the EM-waves at low-band to pass. As shown in Fig. 4 (a), the transmission magnitude is low than 0.1 at 120-GHz and higher than 0.85 at 75-GHz. The transmission phase with and without grid-B is given in Fig. 4 (b). The transmission phase difference between the structure with and without grid-B at 75-GHz is less than 15°. Thus, no additional dielectric layer is added atop of the grid for phase compensating between region II and region IV.

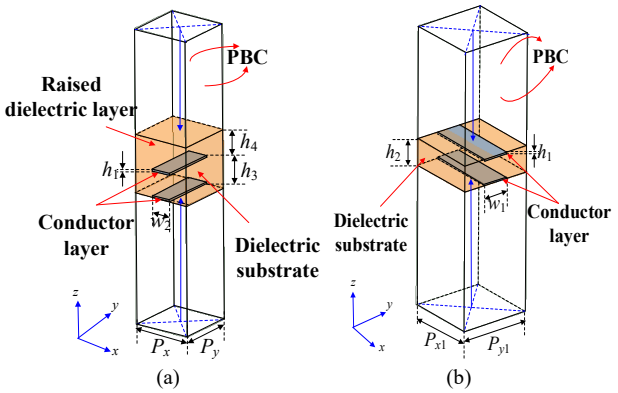

Fig. 2. (a) Grids-A with raised dielectric layer forming region III. (b) Grids-B forming region II. (h_1= 35 μm, h_2= 0.5 mm, h_3= 0.5 mm, h_4= 0.65 mm, w_1= 0.6 mm, w_2= 0.42 mm, P_x =1.2 mm, P_y= 1.2 mm, P_{x1}= 1.7 mm, P_{y1} =1.7 mm)

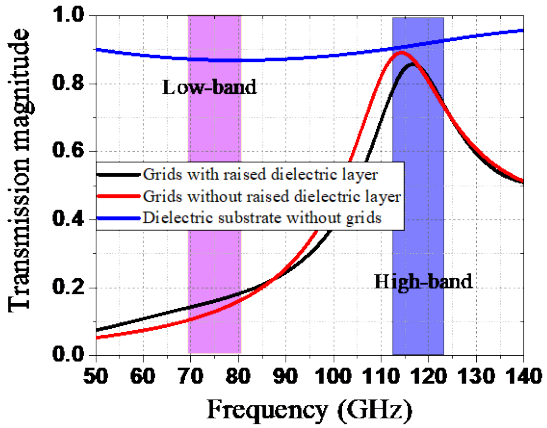

Fig. 3. (a) Simulated transmission magnitude of grid-A with/without raised dielectric layer and dielectric substrate only. (b) Simulated transmission phase of grid-A with/without raised dielectric layer and dielectric substrate only.

C. Dual-band FZP Lens Antenna

The proposed dual-band metalens is simulated in Ansys. HFSS. Because of the symmetry, only one-quarter of the structure is simulated using symmetry boundary conditions. The convergence criteria of adaptive solution in HFSS

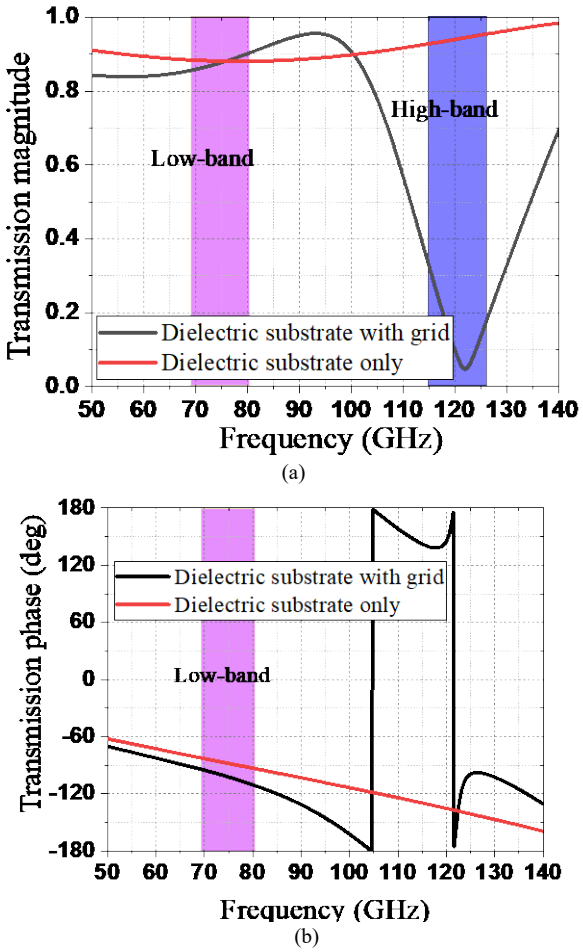

Fig. 4. (a) Simulated transmission magnitude of dielectric with/without grid-B. (b) Simulated transmission phase of dielectric with/without grid-B.

simulation are set to be the maximum Delta S < 0.005 at the two solution frequencies of 75 and 120 GHz. The number of tetrahedral elements is around 2.2×10^5 and 1.1×10^6 at 75 GHz and 120 GHz, respectively. The focal length is set as 30 mm for both bands with a focal to diameter (F/D) ratio of 0.5. The dielectric material is made of ultraviolet (UV) curable acrylates with dielectric constant of 2.8 and loss tangent of 0.02 at 120 GHz. The radiation performance of the dual-band FZP metalens antenna at 75 GHz and 120 GHz are compared with that of the single-band FZP metalens antenna A and B, as shown in Figs. 5 and 6. The radiation patterns of the dual-band FZP metalens antenna and single-band FZP metalens antenna A (B) are nearly the same and the boresight gain differences are less than 1 dB, which demonstrates that two FZP metalens antennas are successfully merged into one dual-band FZP metalens antenna with a shared aperture. Fig. 5. (b) and Fig. 6. (b) also give the radiation patterns and gain comparison between the proposed dual-band FZP metalens antenna with and without raised dielectric layers at high-band, respectively. It is seen from Fig. 5 (b) that, after adding the phase compensating rings, the sidelobe levels of the radiation patterns improved from -6 dB to -12 dB. Meanwhile, the boresight gain improved by 2.4 dB at

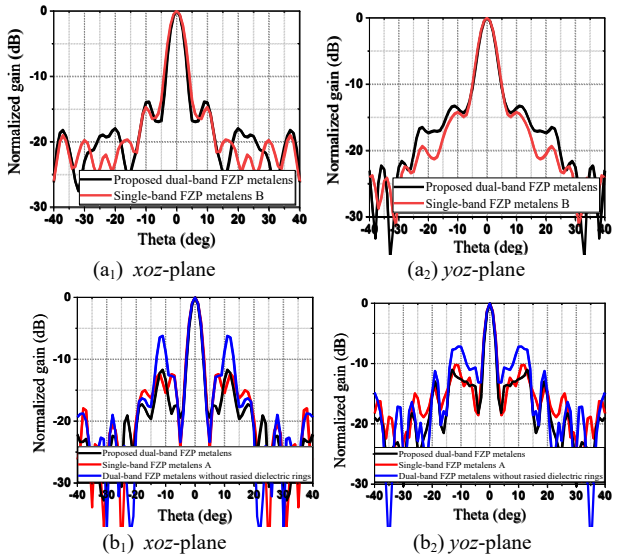

Fig. 5. (a) Radiation performance comparison between the proposed dual-band FZP metalens antenna and the single-band FZP metalens B at 75 GHz (b) Radiation performance comparison between the proposed dual-band FZP metalens antenna and the single-band FZP metalens A at 120 GHz.

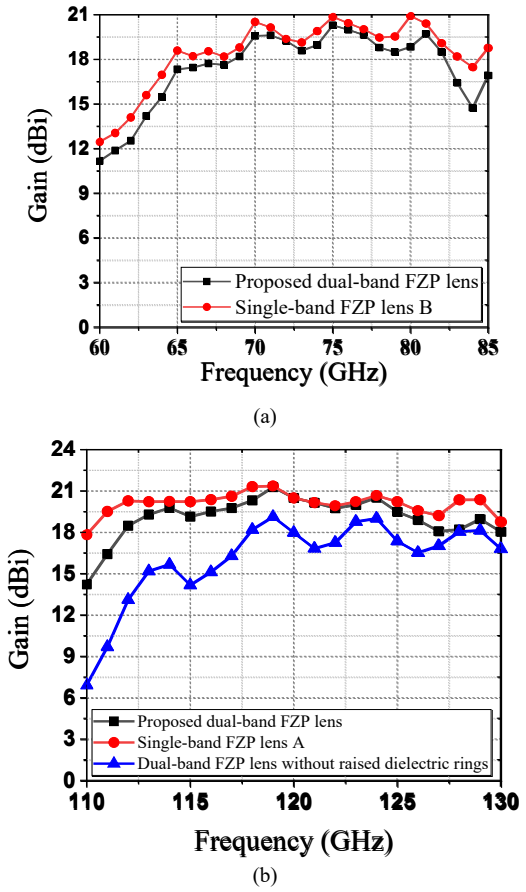

Fig. 6. Boresight gain comparison at two bands. (a) Low-band. (b) High-band.

120-GHz after adding the phase compensating rings, as shown in Fig. 6 (b).

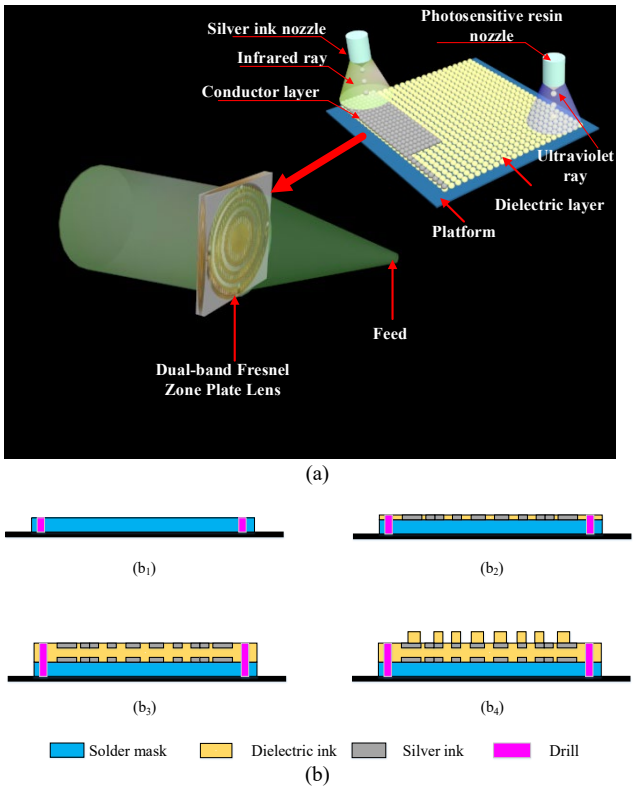

Fig. 7. (a) Proposed dual-band FZP metalens antenna fabricated using integrated conductive/dielectric additive manufacturing. (b) Fabrication steps of the conductive/dielectric one-stop additive manufacturing.

III. Fabrication, Measurement and Discussion

A. AME Fabrication

The prototype is fabricated using DragonFly™ 2020 PRO [49], which has two printing heads for metal and dielectric printing, respectively. Each head consists of 512 piezoelectric based nozzles connecting to an ink-filled chamber (one chamber is filled with silver nanoparticle ink for conductor printing (conductivity of 2×10^7 S/m) and the other is filled with ultraviolet (UV) curable acrylates ink for dielectric printing. An ultrathin dielectric layer is printed first at the bottom as the soldering mask. Then, the dielectric and conductive inks can be simultaneously jetted to form the dielectric and conductive layer (thickness of 35 um) according to the pre-designed patterns. Infrared radiation (IR) lamps and UV lights are turned on to solid the silver ink and curable acrylates ink, respectively, as shown in Fig. 7 (a) and (b). The prototype of the proposed FZP metalens antenna is shown in Fig. 8, which has a circular aperture with a radius of 32.5 mm.

B. Measurement

The radiation performance is measured using a far-field mm-wave measurement system shown in Fig. 9. The signal from the signal generator is up-converted to 75 GHz and 120 GHz through the frequency extension module. Then, the signal is

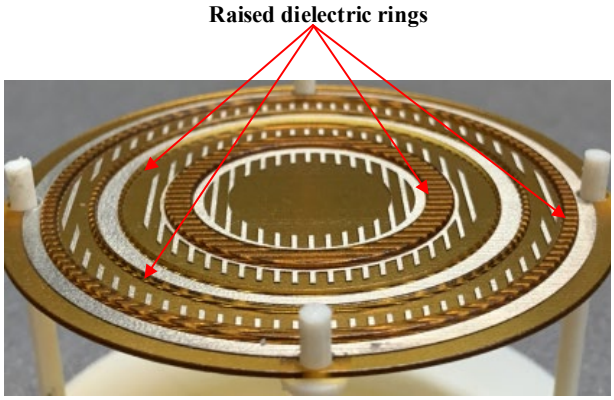

(a)

(b)

Fig. 8. Photographs of the 3D printed metalens antenna: (a) 3-D view. (b) Top view.

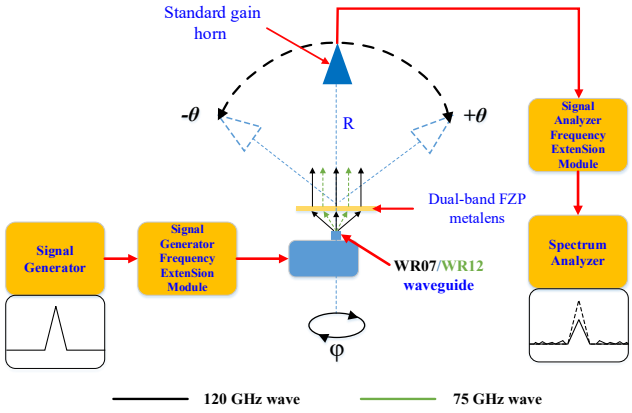

(a)

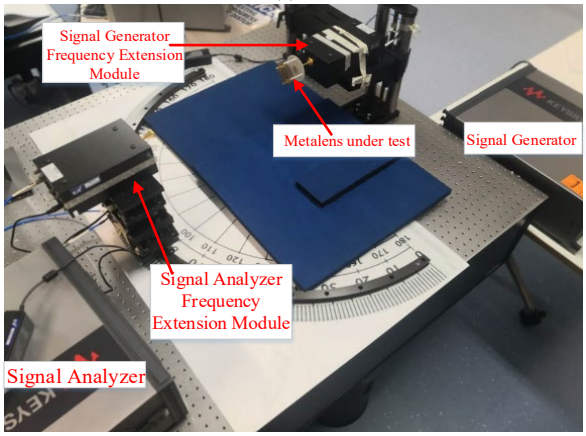

(b)

Fig. 9. (a) Block diagram of the measurement system. (b) Proposed FZP metalens antenna under test.

fed to the dual-band FZP metalens antenna by standard waveguide (WR-12 and WR-07). On the other side, the standard horns are used as the receive antennas at far-field for 75 GHz and 120 GHz, respectively. The receiving horn antenna is connected to a signal analyzer through a frequency extension module. For the gain measurement, two identical standard gain horns are employed for making the direct gain comparison to obtain the gain value. The FZP metalens antenna gain (G_{FZP_lens}) can be obtained by [50]:

$$(G_{FZP\_lens})_{dB} = (G_{horn})_{dB} + 10\log_{10}(\frac{P_{FZP\_lens}}{P_{horn}}) \quad (2)$$

where G_{horn} is the gain of the standard gain horn, P_{horn} is the received power from the standard gain horn, P_{FZP_lens} is the received power from the FZP metalens antenna.

The performance of the proposed dual-band FZP metalens antenna is experimentally verified. The simulated and measured radiation patterns at 75 GHz and 120 GHz are given in Fig. 10 (a) and (b), respectively, which are matched well. The peak gains are fixed at boresight and the sidelobe levels are kept below -10 dB. The simulated and measured gains at two bands are given in Fig. 10 (c). The measured gains are 20.3 dBi at 75 GHz and 21.9 dBi at 120 GHz, respectively. The measurement shows 12.7 dB and 12.9 dB improvement compared to the waveguide source (WR-12 and WR-07), demonstrating the FZP metalens antenna collimate the beams at two bands.

To analyze the ratio of the portions of regions I, II, III, and IV on the radiation performance, two additional cases with different focal lengths of the FZP metalens are simulated since the portions of regions I, II, III, and IV on the aperture depends on the focal length, see Appendix. For case I, the focal lengths are set as 20 mm and 30 mm for 75-GHz and 120-GHz bands, respectively. For case II, the focal lengths are set as 30 mm and 40 mm for 75-GHz and 120-GHz bands, respectively. The results demonstrate that the proposed dual-band FZP metalens solution is still effective when the ratio of the portions of regions I, II, III, and IV changes.

TABLE I
COMPARISON OF STATE-OF-ART FZP LENSES AND OTHER DUAL-BAND LENSES

Ref.	Freq (GHz)	Peak gain	Polarization	Sidelobe level (dB)	Aperture efficiency	Thickness (Normal to the wavelength at low-band)	Fabrication
[23]	Dual-band lens 12.5/14.25 (ratio:1.14)	31/31.8	Dual	-25	45%/41.3%	0.47	PCB
[24]	Dual-band lens 12.5/14.25 (ratio:1.14)	30.2/32.3	Dual	-20	38%/46%	0.48	PCB
[25]	Dual-band lens 19.5/29 (ratio:1.48)	28.1/31	Dual	-20	20.1%/21.2%	0.1	PCB
[26]	Dual-band lens 11/12.5 (ratio:1.14)	23.74/24.45	Dual	-15	38%/34.6%	0.5	PCB
[41]	Single-band focusing FZP lens 32	N.A.	Single	-15	N.A.	0.05	PCB
[44]	Single-band focusing FZP lens 12	N.A.	Single	N.A.	N.A.	0.2	PCB
[45]	Dual-band FZP lens 4.05/5.3 (ratio:1.3)	N.A.	Single	-10	N.A.	0.02	PCB
[46]	Single-band FZP lens 60	32.7	Single	-20	52.8%	9	PCB
[47]	Single-band focusing FZP lens 10	N.A.	Dual	N.A.	N.A.	N.A.	PCB
[52]	Single-band Soret fishnet metalens 96.45	10.64	Single	-15	2%	0.63	PCB
[53]	Single-band Dielectric FZP lens	34.6	Single	-20	52%	1.25	PCB
[54]	Single-band FZP lens 60	27.6	Single	-25	36%	1	Additive manufacturing
[55]	Single-band fishnet metalens 99	20 (simulation) 16.6 (measurement)	Single	-15	3.9% (simulation) 1.8% (measurement)	0.63	PCB
This work	Dual-band FZP lens 75/120 (ratio:1.6)	20.3/21.9	Single	-10	4.8%/2.7%	0.29	Additive manufacturing

IV. DISCUSSION

Table I compares the proposed dual-band FZP metalens antenna with other related works. The general drawback of metallic FZP lens antenna is the low aperture efficiency because it only uses 0/180° phase correction, and 50% energy is reflected [47]. Therefore, for the high gain antenna with high aperture efficiency demand, transmitarray antennas with better phase correcting should be used [23-26], [51]. Nevertheless, to achieve $[-\pi, \pi]$ full phase correcting, the transmitarrays generally require cascading several resonant phasing elements. This can be easily achieved by stacking several PCB layers in order in the microwave region. However, in the mm-wave/THz band, a complicated bonding structure may be required and the cost increases significantly as the number of layers increases. While the metallic FZP lens antenna basically requires only one or two metal layers. Therefore, in some scenarios where antenna layers are restricted, and aperture efficiency is not the primary concern, the FZP lens antenna can be a good substitute for the transmitarray antenna.

Because of the frequency-dependent feature, previous FZP lens antennas are limited to a single-band [41,41,44,46]. Although a reconfigurable dual-band FZP lens is proposed using switch [45], only high gain at one band can generate on the aperture at a given state. In addition, the lossy pin diodes hinder the concept from being applied to the mm-wave regions. Because it is difficult for the phasing element to achieve dual-band/multi-band phase control of the wavefront independently in a single polarization, most of the lenses use polarization to provide a more degree of freedom to realize dual-band [23, 26,47]. In contrast, the proposed ultra-thin FZP metalens antenna can operate at two bands with the same polarization. The radiation performance at the two bands is comparable to that of each single FZP metalens antenna. Regarding the

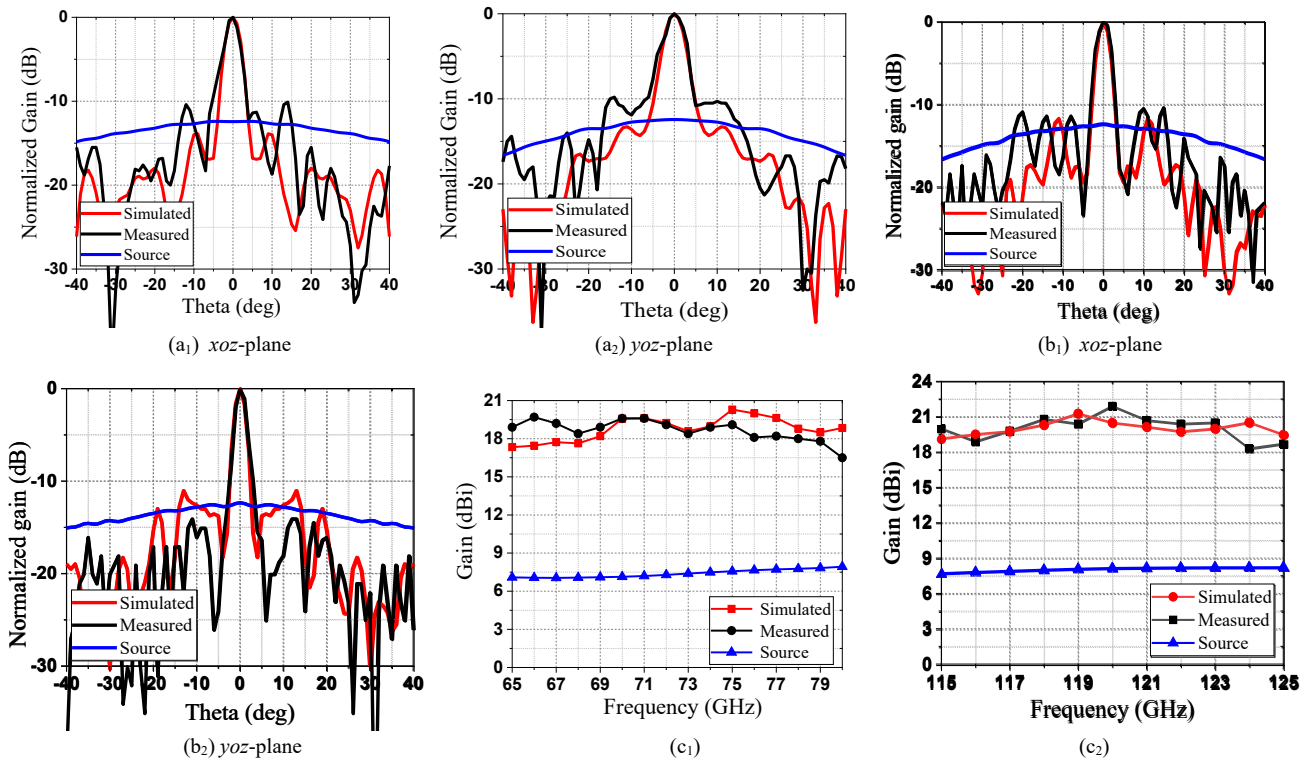

Fig. 10. (a) Simulated and measured radiation patterns at 75 GHz. (b) Simulated and measured radiation patterns at 120 GHz. (c) Simulated and measured boresight gain of the proposed dual-band FZP metalens antenna and the gain of the source at two bands.

frequency ratio, the current unit cells forming the opaque region are suitable for a relatively large frequency ratio. To achieve a very small frequency ratio, unit cells with higher frequency selectivity can be used, but the number of the layers may increase as well.

The general advantage of the dielectric/metal joint printing over PCB fabrication is that: 1) multiple metal layers can be printed in a single dielectric substrate with fewer constraints of the distance between metal layers. 2) No bonding process is required among multiple metal layers. 3) The fabrication cost will not increase as the layer increases. The 3D printing solution provides the designers with more design flexibility than the traditional multi-layer PCB solutions, especially for the designs with small form factor expectations at mm-wave and THz frequencies. Take the proposed design as an example, to compensate for the meta-grids' phase shift, an additional dielectric ring layer is added atop the FZP. The dielectric ring layer can be easily and seamlessly printed on the top of the metallic layer. In contrast, a bonding structure is required if the PCB solution is used. Besides, the distance between the metallic layers and the dielectric layer thickness can be flexibly selected to meet the desired dimensions, which cannot be easily achieved using PCB or low temperature co-fire ceramics (LTCC) solutions.

V. Conclusion

In summary, a shared-aperture dual-band FZP metalens antenna operating at 75GHz and 120 GHz is proposed and experimentally verified. The concentric rings of two FZP metalens antennas made of different kinds of grid polarizers are merged seamlessly, forming the dual-band FZP metalens antenna in a shared aperture. High directional radiation is achieved at two bands with the measured peak gains of 20.3 dBi and 21.9 dBi at 75 GHz and 120 GHz, respectively. The proposed FZP metalens antenna has the merits of the light-weight, low-profile, and fast-prototyped using conductive/dielectric integrated AME technique. Potential applications of the FZP metalens antenna include multi-band mm-wave communications, sensing, and imaging.

Appendix

Two FZP metalenses with different focal lengths are simulated for further demonstration. For case I, the focal lengths are set as 20 mm and 30 mm for 75-GHz and 120-GHz band, respectively. The configuration of the metalens is given in Fig. A1. (a) and the radiation patterns and gain comparison are given in Fig. A1 (b) and (c). For case II, the focal lengths are set as 30 mm and 40 mm for 75-GHz and 120-GHz band, respectively. The configuration of the metalens is given in Fig. 2. A (a) and the radiation patterns and gain comparison are given in Fig. A2 (b) and (c).

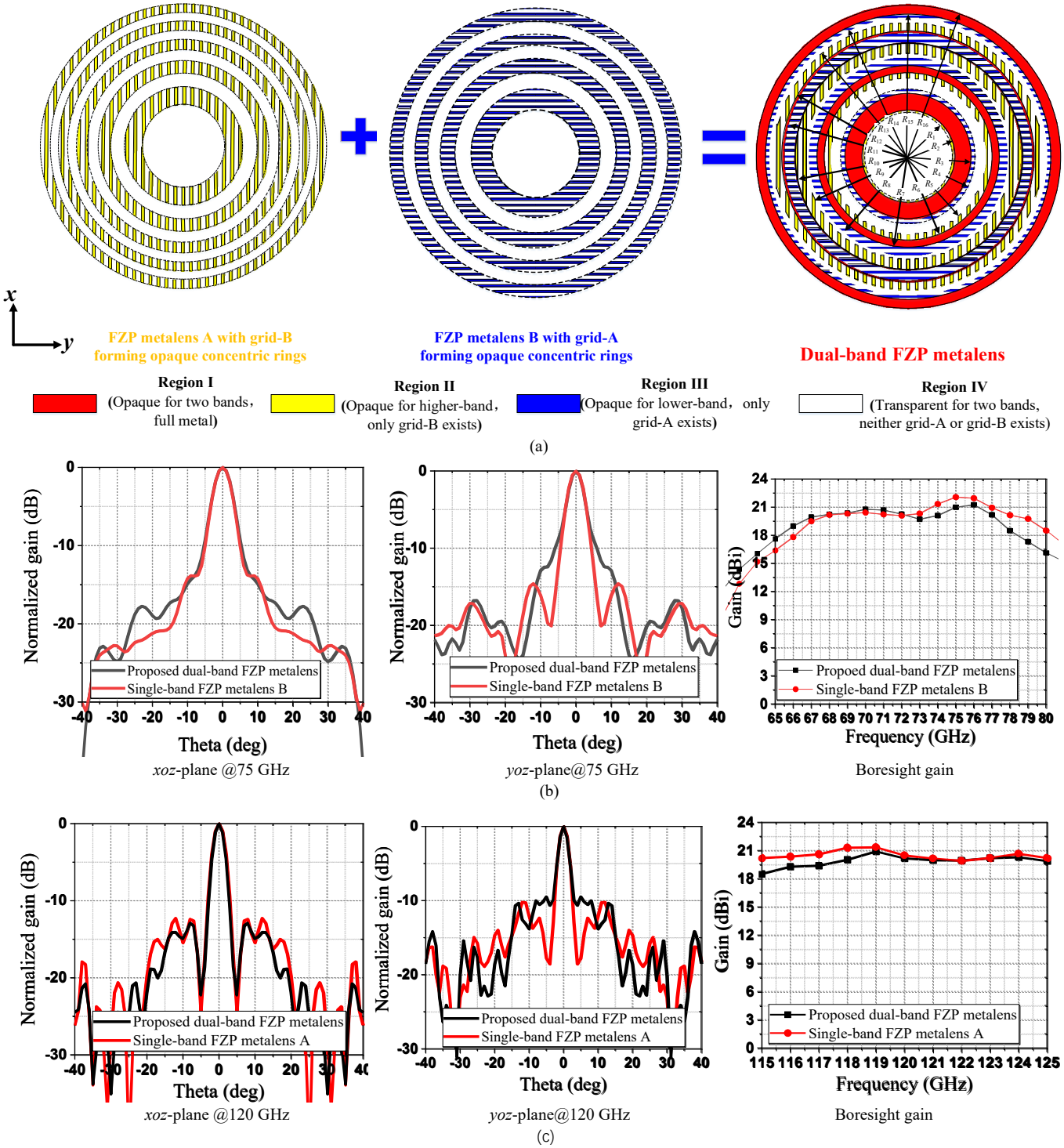

Fig. A1. (a) Configurations of the dual-band FZP meta-lens antenna. Case I: focal length of 20mm at 75-GHz band and 30 mm at 120-GHz band. (FZP metalens A: operating at the high-band and FZP, metalens B: operating at the low-band. R_1= 8.75 mm, R_2=9.16 mm, R_3=12.5 mm, R_4=13.26 mm, R_5=15.46 mm R_6=16.6 mm, R_7=18 mm, R_8=19.6 mm, R_9=20.35 mm, R_{10}=22.5 mm, R_{11}= 24.5 mm, R_{12}=24.9 mm, R_{13}=26.5 mm, R_{14}=27.5 mm, R_{15}= 28.3 mm, R_{16}= 30 mm). (b) Radiation patterns and gain comparison between the proposed dual-band FZP metalens antenna and the single-band FZP metalens B at 75 GHz-band. (c) Radiation patterns and gain comparison between the proposed dual-band FZP metalens antenna and the single-band FZP metalens A at 120-GHz band.

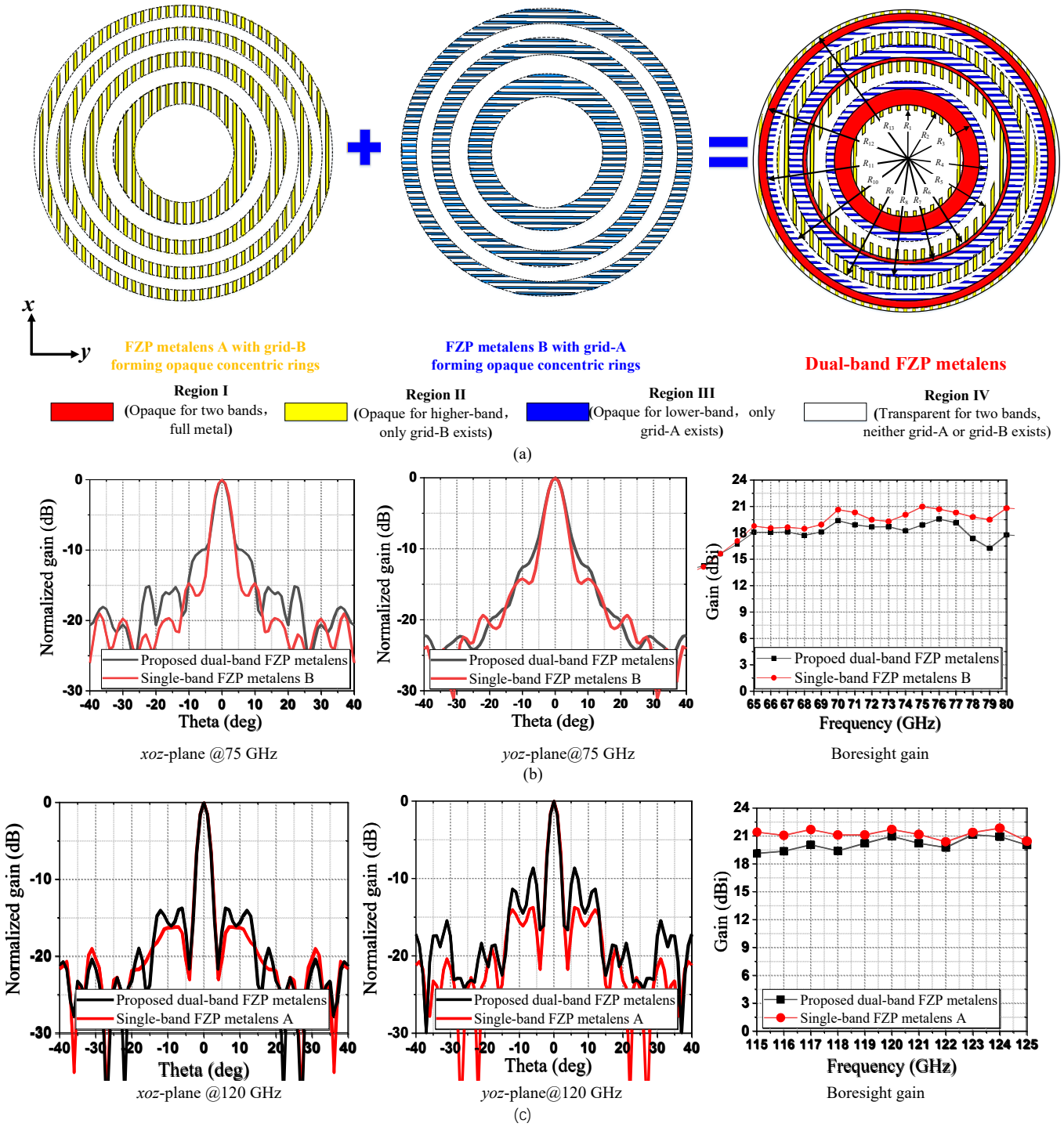

Fig. A2. (a) Configurations of the dual-band FZP metalens antenna. Case II: focal length of 30mm at 75-GHz band and 40 mm at 120-GHz band. (FZP metalens A: operating at the high-band and FZP, metalens B: operating at the low-band. R_1= 10.1 mm, R_2=11.13 mm, R_3=14.36 mm, R_4=16 mm, R_5=17.72 mm, R_6=19.9 mm, R_7=20.61 mm, R_8=23.21 mm, R_9=25.61 mm, R_{10}=26.46 mm, R_{11}= 27.86 mm, R_{12}=29.39 mm, R_{13}=30 mm). (b) Radiation patterns and gain comparison between the proposed dual-band FZP metalens antenna and the single-band FZP metalens B at 75 GHz-band. (c) Radiation patterns and gain comparison between the proposed dual-band FZP metalens antenna and the single-band FZP metalens A at 120-GHz band.

REFERENCE

[1] M. Tonouchi, “Cutting-edge terahertz technology,” *Nat. Photon*., vol. 1, pp. 97–105, 2007.

[2] S. van Berkel, O. Yurduseven, A. Freni, A. Neto and N. Llombart, "THz imaging using uncooled wideband direct detection focal plane arrays," *IEEE Trans. THz Sci. Technol*., vol. 7, no. 5, pp. 481-492, Sept. 2017.

[3] K. B. Cooper, R. J. Dengler, N. Llombart, T. Bryllert, G. Chattopadhyay, E. Schlecht, J. Gill, C. Lee, A. Skalare, I. Mehdi, and P. H. Siegel, “Penetrating 3-D imaging at 4- and 25-m range using a submillimeterwave radar,” *IEEE Trans. Microw. Theory Technol*., vol. 56, no. 12, pp. 2771–2778, Dec. 2008.

[4] R. T. Ako, A. Upadhyay, W. Withayachumnankul, M. Bhaskaran, and S. Sriram, ‘‘Dielectrics for terahertz metasurfaces: Material selection and fabrication techniques,’’ *Adv. Opt. Mater*., vol. 8, no. 3, Feb. 2020, Art. no. 1900750.

[5] H. Song and T. Nagatsuma, "Present and future of terahertz communications," *IEEE Trans. THz Sci. Technol*., vol. 1, no. 1, pp. 256-263, Sept. 2011.

[6] B. Zhang, Y. Guo, H. Zirath and Y. P. Zhang, "Investigation on 3-D-printing technologies for millimeter- wave and terahertz applications," *Proc. IEEE*, vol. 105, no. 4, pp. 723-736, April 2017.

[7] K. Delfanazari, R. A. Klemm, H. J. Joyce, D. A. Ritchie and K. Kadowaki, "Integrated, portable, tunable, and coherent terahertz sources and sensitive detectors based on layered superconductors," *Proc. IEEE*, vol. 108, no. 5, pp. 721-734, May 2020.

[8] D. Headland, Y. Monnai, D. Abbott, C. Fumeaux, and W. Withayachumnankul, “Tutorial: Terahertz beamforming, from concepts to realizations,” *APL Photon*., vol. 3, no. 5, 2018, Art. no. 051101.

[9] W. J. Otter and S. Lucyszyn, "Hybrid 3-D-printing technology for tunable THz applications," *Proc. IEEE*, vol. 105, no. 4, pp. 756-767, April 2017.

[10] T. Kleine-Ostmann and T. Nagatsuma, “A review on terahertz communications research,” *J. Infrared, Millim. Terahertz Waves*, vol. 32, pp. 143–171, 2011.

[11] P. Mei, S. Zhang, X. Q. Lin and G. F. Pedersen, "A millimeter-wave gain-filtering transmitarray antenna design using a hybrid lens," *IEEE Antennas Wireless Propag. Lett*.,, vol. 18, no. 7, pp. 1362-1366, July 2019.

[12] M. Chen, A. Epstein and G. V. Eleftheriades, "Design and experimental verification of a passive huygens’ metasurface lens for gain enhancement of frequency-scanning slotted-waveguide antennas," *IEEE Trans. Antennas Propag*., vol. 67, no. 7, pp. 4678-4692, July 2019.

[13] P. Nayeri, F. Yang, and A.Z. Elsherbeni. Reflectarray antennas: theory, designs, and applications. John Wiley & Sons, 2018.

[14] S. Qu, H. Yi, B. J. Chen, K. B. Ng and C. H. Chan “Terahertz reflecting and transmitting metasurfaces.” *Proc. IEEE*, 2017, 105, no. 6.

[15] S. Liu, Q. Cheng, Q. Xu, T. Q. Wang, L. L. Du, K. Luan, Y. H. Xu, D. Bao, X. J. Fu, J. G. Han, W. L. Zhang, and T. J. Cui, “Free-standing metasurfaces for high-efficiency transmitarrays for controlling terahertz waves.” *Adv. Opt. Mater*., vol. 4, no. 3, pp. 384-390, 2016.

[16] C. Jouanlanne et al., " Wideband linearly polarized transmitarray antenna for 60 ghz backhauling" *IEEE Trans. Antennas Propag*., vol. 65, no. 3, pp. 1440-1445, March 2017.

[17] C. Xue, Q. Lou and Z. N. Chen, " Broadband double-layered huygens' metasurface lens antenna for 5g millimeter-wave systems," *IEEE Trans. Antennas Propag.*, vol. 68, no. 3, pp. 1468-1476, March 2020.

[18] Z. H. Jiang, Y. Zhang, J. Xu, Y. Yu and W. Hong, " Integrated broadband circularly polarized multibeam antennas using berry-phase transmit-arrays for ka -band applications.," *IEEE Trans. Antennas Propag*., vol. 68, no. 2, pp. 859-872, Feb. 2020.

[19] S. L. Liu, X. Q. Lin, Z. Q. Yang, Y. J. Chen and J. W. Yu, " w-band low-profile transmitarray antenna using different types of fss units," *IEEE Trans. Antennas Propag*., vol. 66, no. 9, pp. 4613-4619, Sept. 2018.

[20] M. Jiang, Z. N. Chen, Y. Zhang, W. Hong and X. Xuan, " Metamaterial-based thin planar lens antenna for spatial beamforming and multibeam massive mimo," *IEEE Trans. Antennas Propag*., vol. 65, no. 2, pp. 464-472, Feb. 2017.

[21] J. Wang et al., " Metantenna: when metasurface meets antenna again," *IEEE Trans. Antennas Propag*., vol. 68, no. 3, pp. 1332-1347, March 2020.

[22] Z. Shi, S. Yang, S.-W. Qu, and Y. Chen, “Circularly polarised planar Luneberg lens antenna for mm-Wave wireless communication,” *Electron. Lett*., vol. 52, no. 15, pp. 1281–1282, 2016.

[23] A. Aziz, F. Yang, S. Xu and M. Li, " An efficient dual-band orthogonally polarized transmitarray design using three-dipole elements.," *IEEE Antennas Wireless Propag. Lett*., vol. 17, no. 2, pp. 319-322, Feb. 2018.

[24] A. Aziz, F. Yang, S. Xu, M. Li and H. Chen, " A high gain dual-band and dual-polarized transmitarray using novel loop elements," *IEEE Antennas Wireless Propag. Lett.*, vol. 18, no. 6, pp. 1213-1217, June 2019.

[25] K. T. Pham, R. Sauleau, E. Fourn, F. Diaby, A. Clemente and L. Dussopt, " Dual-band transmitarrays with dual-linear polarization at ka-band. Antennas and Propagation," *IEEE Trans. Antennas Propag*., vol. 65, no. 12, pp. 7009-7018, Dec. 2017.

[26] M. O. Bagheri, H. R. Hassani and B. Rahmati, "Dual-band, dual-polarised metallic slot transmitarray antenna," *IET Microw., Antennas Propag*., vol. 11, no. 3, pp. 402-409, 2017.

[27] C. Wang, J. Wu and Y. Guo, " A 3d-printed multibeam dual circularly polarized luneburg lens antenna based on quasi-icosahedron models for ka-band wireless applications" *IEEE Trans. Antennas Propag*, vol. 68, no. 8, pp. 5807-5815, Aug. 2020.

[28] M. F. Farooqui and A. Shamim, "3-D inkjet-printed helical antenna with integrated lens," *IEEE Antennas Wireless Propag. Lett*., vol. 16, pp. 800-803, 2017.

[29] H. Yi, S. Qu, K. Ng, C. H. Chan and X. Bai, "3-d printed millimeter-wave and terahertz lenses with fixed and frequency scanned beam.," *IEEE Trans. Antennas Propag*., vol. 64, no. 2, pp. 442-449, Feb. 2016.

[30] A. C. Paolella, C. D. Fisher, C. Corey, D. Foster and D. Silva-Saez, "3-D Printed Millimeter-Wave Lens Systems at 39 GHz," *IEEE Microw. Wireless Compon. Lett*., vol. 28, no. 6, pp. 464-466, June 2018.

[31] G. Wu, Y. Zeng, K. F. Chan, S. Qu and C. H. Chan, "33-d printed circularly polarized modified fresnel lens operating at terahertz frequencies," *IEEE Trans. Antennas Propag.*, vol. 67, no. 7, pp. 4429-4437, July 2019.

[32] B. Zhang et al., " A k-band 3d printed focal-shifted two-dimensional beam scanning lens antenna with non-uniform feed," *IEEE Antennas Wireless Propag. Lett*.,, vol. 18, no. 12, pp. 2721-2725, Dec. 2019.

[33] Y. Li, L. Ge, M. Chen, Z. Zhang, Z. Li and J. Wang, " Multibeam 3-d-printed luneburg lens fed by magnetoelectric dipole antennas for millimeter-wave mimo applications," *IEEE Trans. Antennas Propag*., vol. 67, no. 5, pp. 2923-2933, May 2019.

[34] J. M. Monkevich and G. P. Le Sage, "Design and Fabrication of a Custom-Dielectric Fresnel Multi-Zone Plate Lens Antenna Using Additive Manufacturing Techniques," *IEEE Access*, vol. 7, pp. 61452-61460, 2019.

[35] J. Budhu and Y. Rahmat-Samii, "3D-Printed Inhomogeneous Dielectric Lens Antenna Diagnostics: A Tool for Assessing Lenses Misprinted Due to Fabrication Tolerances," *IEEE Antennas Propag. Mag*, vol. 62, no. 4, pp. 49-61, Aug. 2020.

[36] J. Zhu et al., "3-D printed planar dielectric linear-to-circular polarization conversion and beam-shaping lenses using coding polarizer," *IEEE Trans. Antennas Propag*., vol. 68, no. 6, pp. 4332-4343, June 2020.

[37] M. K. T. Al-Nuaimi and W. Hong, " Discrete dielectric reflectarray and lens for e-band with different feed" *IEEE Antennas Wireless Propag. Lett.,* vol. 13, pp. 947-950, May, 2014.

[38] K. X. Wang and H. Wong, " Design of a wideband circularly-polarized millimeter wave antenna with an extended hemispherical lens," *IEEE Trans. Antennas Propag*., vol. 66, no. 8, pp. 4303-4308, Aug. 2018.

[39] H. Xin and M. Liang, "3-d-printed microwave and thz devices using polymer jetting techniques," *Proc. IEEE*, vol. 105, no. 4, pp. 737-755, April 2017.

[40] H. Qiao et al., "Compact terahertz detector based on lightweight 3D-printed lens packaging," *Electron. Lett*., vol. 55, no. 14, pp. 796-797, 2019.

[41] S. Karimkashi, A.A. Kishk, “Focusing properties of fresnel zone plate lens antennas in the near-field region,” *IEEE Trans. Antennas Propag*., vol. 59, no. 5, pp. 1481-1487, May 2011.

[42] H.D. Hristov, L.P. Kamburov, J.R. Urumov, R. Feick, “Focusing characteristics of curvilinear half-open fresnel zone plate lenses: plane wave illumination.” *IEEE Trans. Antennas Propag*., vol. 53, no. 6, pp. 1912-1919, June 2005.

[43] H. D. Hristov, Fresnel Zones in Wireless Links, Zone Plate Lenses, and Antennas. Boston, MA: Artech House, 2000.

[44] Y. Fan, B.-L. Ooi, H.D. Hristov, M.-S. Leong, “Compound diffractive lens consisting of fresnel zone plate and frequency selective screen,” *IEEE Trans. Antennas Propag.*, vol. 58, no. 6, pp. 1842-1847, June 2010.

[45] H. Li, C. Ma, D. Ye, Y. Sun, W. Zhu, C. Li, and L. Ran, “Dual-band fresnel zone plate antenna with independently steerable beams” *IEEE Trans. Antennas Propag*., vol. 66, no. 4, pp. 2113-2118, April 2018.

[46] M. R. Dehghani Kodnoeih, Y. Letestu, R. Sauleau, E. Motta Cruz and A. Doll, " Compact folded fresnel zone plate lens antenna for mm-wave communications," *IEEE Antennas Wireless Propag. Lett*., vol. 17, no. 5, pp. 873-876, May 2018.
[47] H. Markovich, D. Filonov, I. Shishkin and P. Ginzburg, "Bifocal fresnel lens based on the polarization-sensitive metasurface," *IEEE Trans. Antennas Propag.*, vol. 66, no. 5, pp. 2650-2654, May 2018.
[48] A. F. Kurtz, R. Sujatha, & M. I. Xiang-Dong, "Wire grid polarizer," U.S. Patent. No. 6,665,119.16 Dec. 2003.
[49] DragonFly LDM® Lights-Out Digital Manufacturing system https://www.nano-di.com/ame-dragonfly-ldm, accessed on 10 April 2021.
[50] C. A. Balanis, Antenna Theory Analysis and Design. New York: Wiley, 1997.
[51] S. A. Matos et al., "High gain dual-band beam-steering transmit array for satcom terminals at Ka-Band," *IEEE Trans. Antennas Propag*., vol. 65, no. 7, pp. 3528–3539, Jul. 2017.
[52] B. Orazbayev, M. Beruete, V. Pacheco-Peña, G. Crespo, J. Teniente, and M. Navarro-Cía, "Soret fishnet metalens antenna," *Sci. Rep*., vol. 5, May 2015, Art. no. 9988.
[53] A. Jouade, J. Bor, M. Himdi, and O. Lafond, "Millimeter-wave Fresnel zone plate lens with new technological process*," Int. J. Microw. Wireless Technol.*, vol. 9, no. 4, pp. 939–944, 2017.
[54] J. Pourahmadazar and T. A. Denidni, "Towards millimeter-wavelength: transmission-mode Fresnel-zone plate lens antennas using plastic material porosity control in homogeneous medium," *Sci. Rep*., vol. 8, no. 5300, pp. 1–14, Mar. 2018.
[55] B. Orazbayev, M. Beruete, and M. Navarro-Cía, "Wood zone plate fishnet metalens," *EPJ Appl. Metamaterials*, vol. 2, p. 8, 2015.

Jianfeng Zhu was born in Changsha, China. He received the B. Eng. degree in communication engineering from Beijing University of Posts and Telecommunications (BUPT), Beijing, China, in 2013 and currently pursuing the joint Ph. D. degree with BUPT and University of Technology Sydney (UTS), Ultimo, NSW, Australia. From Nov. 2015 to Jun. 2018, he was research assistant with the State Key Laboratory of Millimeter Waves, Department of Electronic Engineering, City University of Hong Kong. Since 2018, he is a visiting scholar with South China University of Technology (SCUT) with the research of LTCC and antenna-in-package. He has authored and coauthored more than 40 journal and conference articles. His current research includes THz/SubTHz beam shaping and 3-D printing.

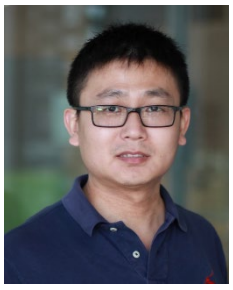

Dr. Yang Yang (S'11–M'14-SM'17) was born in Bayan Nur and grew up in Hohhot, Inner Mongolia, China. He received the MEng, MSc, and PhD degrees from Department of Electrical and Computer Systems Engineering (ECSE) in Clayton Campus, Monash University, Melbourne, Australia, in 2007, 2008 and 2013, respectively.

Dr. Yang has three years industry experience at Rain Bird Australia serving as an Asia Pacific GSP Engineer, during 2012 to 2015. He received the corporate 2014 Global GSP Success Award (one globally). In April 2015, he returned to academia and served as a Senior Research Associate with the Centre for Collaboration in Electromagnetic and Antenna Engineering at Macquarie University. In April 2016, he was appointed as a Research Fellow with State Key Laboratory of Terahertz and Millimeter Waves, City University of Hong Kong. Since December 2016, Dr. Yang joined University of Technology Sydney, Australia. He is currently a Senior Lecturer and a team leader of Millimetre-Wave Integrated Circuits and Antennas. His research interests include millimetre-wave and sub-terahertz technologies in 5G and biomedical applications. He has over 150 international peer reviewed publications in microwave and millimetre-wave circuits and antennas.

Dr Yang is a current Associate Editor of *IEEE ACCESS*, and an Area Editor (Track Editor) of *MICROWAVE AND OPTICAL TECHNOLOGY LETTERS*. He is a current committee member of MTT-28 Biological Effects and Medical Applications. Dr Yang is a winner of CST University Publication Award 2018, by CST, Dassault Systèmes.

Mengze Li was born in Hunan, China, in 1994. She received the B.Eng. degree in electrical engineering and automation from Hunan University, Hunan, China, in 2015. And She received the M.Eng. degree in Electronic Field and Microwave Technology in Xiamen University, Xiamen, China, in 2018. From 2017 to 2018, she was a Visiting Student with the Faculty of Engineering and Information Technology, University of Technology Sydney, Australia, where she is currently pursuing the Ph.D. degree. Her current research interests include microstrip filters, multiplexers, RFIC and 3-D Print technology.

Professor David McGloin received a MSci (Hons) degree in Laser Physics and Optoelectronics and a PhD degree in Laser and Atomic Physics from the University of St. Andrews in the UK in 1997 and 2001 respectively. He worked for the UK Defence Science and Technology Laboratory at Fort Halstead before taking up a postdoctoral research fellowship in atom optics at St. Andrews in 2002. He was awarded a Royal Society University Research Fellowship from 2003 to 2011. He was a visiting scholar at the University of Washington in Seattle in 2006. He took up a lectureship in the Division of Physics at the University of Dundee in the UK in 2007 and subsequently was a Senior Lecturer and Reader. He was also Head of Physics and the Associate Dean for Research in the School of Science and Engineering at Dundee. He joined UTS in Sydney in 2018 as a Professor of Optical Physics and Director of

Research Programs in the Faculty of Engineering and IT. His current research interests include optical trapping and manipulation, optical and THz beam shaping, aerosol science, biophotonics, microscopy and Raman spectroscopy. He has published more than 80 peer reviewed papers, is a Senior Member of the Optical Society of America and a Member of the Institute of Physics.

Shaowei Liao (M'13–SM'16) received the Ph.D. degree in electromagnetic fields and microwave technology from the University of Electronic Science and Technology of China (UESTC), Chengdu, China, in 2010. In 2011, he joined the School of Electronic Engineering, UESTC, as a Lecturer. From 2011 to 2012, he was a Senior Research Associate with the Department of Electronic Engineering, City University of Hong Kong, Hong Kong. From 2012 to 2013, he was a Research Scientist with Bell Labs Research, Shanghai Bell, Alcatel-Lucent, China. From 2013 to 2017, he was an Engineer with the State Key Laboratory of Millimeter Waves, City University of Hong Kong. He is currently an Associate Professor with the School of Electronics and Information Engineering, South China University of Technology. He has authored or co-authored more than 30 papers on IEEE journals. He is a co-inventor of five granted U.S. and European patents. His current research interests include various antennas, microwave components, and computational electromagnetics.

Dr. Liao is a reviewer for the IEEE TRANSACTIONSON ANTENNAS AND PROPAGATION, the IEEE ANTENNAS AND WIRELESS PROPAGATION LETTERS, and the IEEE MICROWAVEAND WIRELESSCOMPONENTSLETTERS. He is the winner of 2017 H. A. Wheeler Applications Prize Paper Award.

Dr. Jaim Nulman received an undergraduate degree from Technion-Israel Institute of Technology in 1979, a master degree in 1982 and a doctorate in 1984 from Cornell University, all in Electrical Engineering, and an MBA from Stanford University in 1994. He is a proven influencer and innovator with more than 30 years of expertise in working with companies from start-ups to Fortune 500 enterprises. He served as Vice President of Applied Materials, where he spent 15 years in several product division and corporate positions. He drove the successful commercialization of one of Applied Materials' semiconductor manufacturing products with impressive market penetration of $1 billion in less than five years. He is a co-inventor in over 30 patents in the area of semiconductor manufacturing technology, semiconductor manufacturing equipment, and additive manufacturing for electronics. He has served as invited lecturer at UC Berkeley extension, and NATO's International Summer Institute.

Minoru Yamada was born in Toyama, Japan, in 1952. He was involved the Electronics product development more than 40 years especially wireless telecommunication products such as voice and video data transfer system using DECT technology. He was developed more than 50 products and sold in market under British telecom, Motorola, Philips, Uniden, Telstra and some others brands. His responsibility was mainly RF hardware and software development. Last 20 years were mainly managing the R&D department and product architecture development.

Professor Francesca Iacopi has over 20 years' international industrial and academic expertise in the miniaturisation of semiconductor technologies. She has led large R&D projects for IMEC (Belgium) and Globalfoundries Inc (USA) in interconnects, electronic devices and packaging. Her focus is the translation of basic scientific advances into nanomaterials and device concepts into integrated technologies. She is known for her work in porous dielectrics for interconnects, and, more recently, graphene for on-chip applications. She is a recipient of an MRS Gold Graduate Student Award (2003), an ARC Future Fellowship (2012), and a Global Innovation Award in Washington DC (2014), she was listed among the most innovative engineers by Engineers Australia (2018). Francesca is a Fellow of the Institution of Engineers Australia and currently serves in several technical committees for the Materials Research Society, the IEEE Electron Devices Society, as well as the International Roadmap for Systems and Devices. She leads the Integrated Nanosystems Lab, in the Faculty of Engineering and IT, University of Technology Sydney and is a Chief Investigator of the ARC Centre of Excellence in Transformative Meta-Optical Systems (TMOS).